Published in final edited form as:
Ultrasound Med Biol. 2019 August ; 45(8): 2075–2085. doi:10.1016/j.ultrasmedbio.2019.05.002.

Myocardial Fiber Mapping of Rat Hearts Using Apparent Backscatter, with Histological Validation

Michelle L Milne[1], **Brianna M. Schick**[2], **Thamer Alkhazal**[2], and **Charles S Chung**[2]

[1]Department of Physics, St Mary's College of Maryland, St Mary's City MD USA

[2]Department of Physiology, Wayne State University, Detroit MI USA

Abstract

Myocardial fiber architecture is a physiologically important regulator of ejection fraction, strain, and pressure development. Apparent ultrasonic backscatter has been shown to be a useful method for recreating the myocardial fiber architecture in human-sized sheep hearts, due to the dependence of its amplitude on the relative orientation of a myofiber to the angle of ultrasonic insonification. Thus, the anisotropy of the backscatter signal is linked to, and provides information about, the fiber orientation. In this study, we sought to determine if apparent backscatter could be used to measure myofiber orientation in rodent hearts. Fixed adult rat hearts were imaged intact, and both a transmural cylindrical core and transmural wedge of the LV free wall were imaged. Cylindrical core samples confirmed that backscatter anisotropy could be measured in rat hearts. Ultrasound and histological analysis of transmural myocardial wedge samples confirmed that the apparent backscatter could be reproducibly mapped to fiber orientation (angle of the fiber relative to the direction of insonification). These data provided a quantitative relationship between the apparent backscatter and fiber angle that was applied to whole heart images. Myocardial fiber architecture was successfully measured in rat hearts. Quantifying myocardial fiber architecture using apparent backscatter provides a number of advantages, including its scalable use from rodents to man, its rapid low-cost acquisition, and minimal contraindications. The method outlined in this study provides a method for investigators to begin detailed assessments of how the myocardial fiber architecture changes in pre-clinical disease models, which can be immediately translated into the clinic.

Keywords

Ultrasound tissue characterization; Anisotropy; Myocardial; Apparent Backscatter

Corresponding Author Charles S Chung, PhD, Department of Physiology, Wayne State University, 5374 Scott Hall, 540 E Canfield, Detroit MI 48201, cchung@med.wayne.edu, Tel: (313) 577-1540, Fax: (313) 577-5494.

DISCLOSURES
None

Health Research Alliance Author Manuscript

INTRODUCTION

Standard echocardiographic indexes of cardiac function (such as wall thickness, E' and A' indicating mitral annulus velocity) implicitly assume that the left ventricle (LV) is homogenous (Buckberg, et al. 2008). However, the left ventricle is an anisotropic "weave" of cardiac fibers that begins as a right-hand helix at the epicardium, transitions to circumferential in the mid-myocardium, and transitions into a left-hand helix at the endocardium (Kocica, et al. 2006, Streeter and Hanna 1973). Change in myocardial fiber architecture is correlated with progression of cardiac disease (von Deuster, et al. 2016), suggesting that tracking progressive changes in fiber architecture may be of value (Mizuguchi, et al. 2008).

The underlying LV myocardial fiber (myofiber) architecture defines the maximum ejection fraction and modifies pressure generation. A helical (spiral) architecture is required to generate normal healthy ejection fractions of 60–80% because myofibers only shorten by approximately 15% or less (Ingels 1997, Sallin 1969, Streeter and Hanna 1973). The spiral and counter-spiral of the subendo- and subepicardial myofibers function to generate twist, while the circumferentially aligned mid-myocardial fibers optimize the transfer of myofiber tension into LV pressure (minimum radius via LaPlace's Law) (Ingels 1997). Thus, cardiac indexes such as ejection fraction and torsion are the result of the anisotropic myofiber architecture of the heart. Importantly, cardiac activation may modify the alignment of myofibers between diastolic and systolic periods (Buckberg, et al. 2004).

The availability of pre-clinical rodent models of disease establishes a need to monitor myocardial fiber orientation in the rodent heart. Diffusion tensor magnetic resonance imaging (DTI) is perhaps the most established non-invasive technique used to image myocardial fiber architecture. Current state of the art does allow DTI techniques to be used to map the myofiber architecture throughout the cardiac cycle in humans (Stoeck, et al. 2014, von Deuster, et al. 2016). However, the spatial and temporal resolution for this technique makes monitoring of fiber architecture in rodents both cost- and time-prohibitive.

Previously, the fiber orientation (angle of the fiber relative to the direction of insonification) of human-sized sheep heart was determined using ultrasound and validated using DTI (Milne, et al. 2012, Milne, et al. 2016). The method utilizes a change in apparent ultrasonic backscatter that is dependent on the orientation of myofibers. Myofibers that are perpendicular to the angle of ultrasonic insonification produce larger backscatter compared to myofibers that are parallel. This previous work showed that clinical-frequency ultrasound could be used to map myocardial fiber architecture in large animals. However, it is unclear if apparent backscatter can be used in rodents to evaluate myofiber orientation, not the least because of the low-resolution of clinical imaging systems.

In this study, we used high-frequency ultrasound to determine the myofiber architecture in rat hearts. We established the relationship between backscatter intensity and fiber angle in the rodent hearts and validated this relationship using histology. Advances using this method may provide pre-clinical researchers a rapid, cost-effective method to monitor remodeling of myocardial fiber architecture in rodent models of disease.

METHODS

Animals

Nine female Sprague Dawley rats (Charles River; age: 3.6 ± 1.3 months, body weight: 256±6 g) were used for this study. All procedures were approved by the Wayne State University Institutional Animal Care and Use Committee and follow NIH Guidelines for the care and use of Animals.

Fixed hearts

Seven hearts were obtained from rats anesthetized under 3% isoflurane. Hearts were rapidly isolated, rinsed in cold (4ºC) Perfusion Buffer [in mM: 113 NaCl, 4.7 kCl, 0.6 KH_2PO_4, 0.6 Na_2HPO_4, 1.2 $MgSO_4$, 12 NaHCO3, 10 KHCO3, 10 HEPES (4-(2-hydroxyethyl)-1-piperazineethanesulfonic acid), 30 taurine, 5mM glucose, 10 BDM (2 3-butanedione monoxime)], cannulated, and Langendorff perfused with Perfusion Buffer at constant pressure (70 cmH_2O). After running clear, perfusion was changed to Fixation Buffer (Perfusion Buffer with 2% glutaraldehyde). The heart was fixed under Langendorff perfusion for a minimum of 15 minutes. The heart was then removed and post-fixed in Fixation Buffer for a minimum of 48 hours. The heart was washed three times with PBS [in mM: 10 Phosphate Buffer, 2.7 KCl, 137 NaCl] and stored in PBS at 4ºC until use as described below (Figure 1, step A).

Ultrasound System and Settings

This study utilized an MS250D transducer (21Mhz center frequency, 8mm geometric focus) attached to a VisualSonics Vevo2100 (FujiFilm VisualSonics, Toronto ON) small animal ultrasound system. We determined the transmit power and receiver gain settings for which the mean apparent backscatter intensity vs gain was linear (Kovacs, et al. 2004) using a consumer grade sponge, 2% agarose phantom, and fixed cardiac tissue. Both standard imaging and RF-Mode imaging were acquired when available. Transmit power did not influence linearity; receiver gain provided linearity in a range of roughly 45–65 dB. Using this information, we set transmit power to 100% and receiver gain to 55 dB or 60 dB. Time gain compensation (TGC) was set to zero at all levels. Dynamic range was set at 65 dB, but did not impact our analysis because RAW data output was used for apparent backscatter intensity data. The RAW data represents a log-compressed envelope of the in-phase and quadrature (IQ) radiofrequency data signal after gain and TGC settings are applied, but before dynamic range is applied and displayed on screen. (Dynamic range settings do impact exported Tagged Image File Format images, but nearly identical outputs are observed across a number of dynamic range settings using the built-in C5 Display (color) Map with all TGC levels set to zero.)

Experiment 1 - Core Imaging to Obtain Quantitative Angle-to-Backscatter Relationship

Transmural cylindrical core samples were used to quantify the relationship between fiber angle and apparent ultrasonic backscatter intensity as in a previous study (Milne, et al. 2012). Core samples of 2 or 3 mm in diameter were obtained from the LV free wall of the fixed hearts (Figure 1, steps D, E). The tissue was submerged in PBS and mounted on a

rotating stage perpendicular to the transducer. The cylindrical samples were centered near the focal plane of the transducer in the mid-myocardium. B-mode images of each core were acquired in 5º increments around a full 360º rotation a static imaging plane (transmural depth) using both standard and RF-Mode acquisition.

Images were exported using VevoLab (FujiFilm VisualSonics, Toronto ON) as standard 8-bit (without RF-mode) or 32-bit (with RF-mode) RAW files. Apparent backscatter intensity was determined using a custom MATLAB (MathWorks, Natick MA) script for each core in each mode. Data for each heart and mode were then aligned to their peaks (assumed to be perpendicular insonification, e.g. 90º or 270º) and troughs (assumed to be parallel insonification, e.g. 0º or 180º). Data was averaged to create a single 0–180 degree segment for each core to find a relationship between backscatter and rotation angle (i.e. the backscatter values for 10 degrees and 190 degrees were averaged, 20 degrees and 200 degrees were averaged, etc.). Mean and standard deviation of each of the seven hearts were calculated for each data acquisition mode. Previous work indicated that the relationship between apparent backscatter and fiber angle may be empirically modeled by a function of even powers of sines and cosines (Milne, et al. 2012, Milne, et al. 2016, Mottley and Miller 1988). Based on these works and our fits of individual and mean data, the mean data was fit to the following function:

$$I(\theta) = C_1 + C_2 \bullet \sin^6\theta + C_3 \bullet \cos^6\theta \quad \{\text{Eq. 1}\}$$

where I is the intensity of the apparent ultrasonic backscatter, C_n are constants, and θ is the relative angle between the myofiber orientation and the insonification direction for each mode.

Experiment 2 - Ultrasound and Histological Imaging of Myocardial Segments

Small (approximately 2 mm by 2 mm) trapezoidal segments were obtained from each heart. Segments were obtained using a matrix slicer (Zivic Instruments, Pittsburgh, PA) by first isolating a 2mm thick radial (cylindrical) slice, then making non-parallel cuts using a razor blade (Figure 1, steps C–F). Each tissues segment was submerged in PBS and aligned perpendicular to the imaging surface of the transducer. Serial B-mode images were acquired in 100μm steps from the epicardium to the endocardium, using only standard (without-RF mode) imaging. The tissue was then removed and stored at 4°C. The images were exported using VevoLab Software as 8-bit RAW files. A custom MATLAB script was used to quantify the RAW apparent backscatter intensity at the center of the segment and the relative orientation of the tissue segment, which was roughly perpendicular to the long axis of the heart.

A cryostat (Microm HM550, ThermoScientific, Kalamazoo MI) was used to quantify myocardial fiber orientation. Each previously imaged segment was embedded in Tissue-Tek O.C.T. Compund (Sakura Finteck USA) using a 10mm diameter cryo-mold on a sample stage. The tissue was placed epicardium-outward and the cryostat blade was aligned to cut parallel to the epicardial surface. 50 μm thick serial sections were obtained and were adhered

to a microscope slide in the order they were obtained. After obtaining all sections, each slice was imaged under a microscope (Nikon Eclipse Ci, Nikon Instruments Inc, Melville, NY) using a 2x objective and a 10 megapixel camera (MU1003-CK, AmScope, Irvine CA) mounted in the microscope's eyepiece. A custom MATLAB script was used to manually determine the fiber orientation near the center of the slice relative to the side of the segment that was roughly perpendicular to the long axis of the heart. Briefly, a reference line was created along the top of the muscle segment that corresponded to the top of the segment in the ultrasound image. Two fibers were then manually traced near the middle of the sample, where backscatter analysis would also be performed. The relative histological angle was calculated. Slices with folds, curves, tears, or large vascular pockets were not used. To determine the relative fiber angle transmurally through the myocardium, the tissue thickness (not including clear papillary muscle segments) was normalized. Data were averaged in segments accounting for 5% of the transmural thickness for each heart.

Ultrasound images were interpolated (nearest-neighbor average) to obtain 50 μm steps. Histology and backscatter images were manually aligned and rotated. Apparent backscatter data were averaged in 5 degree bins, based on the histologically determined angle. The relationship between backscatter [dB] and angle were averaged, fit independently to Eq. 1, and compared to the fit of the core data above to provide validation of the core fit.

Experiment 3 - Whole Heart Imaging

Before core or trapezoidal tissue segments (Experiments 1 and 2 above) were obtained, whole heart imaging was performed in four of the seven hearts. Each heart was submerged in PBS, apex upwards towards the transducer (Figure 1, step B). The focal point of the ultrasonic transducer was centered approximately halfway between the base and apex of the heart. The heart was imaged in B-mode using only RF-Mode acquisition with the settings delineated above as it was rotated in 10º increments. The images were exported as 32-bit RAW files and processed using a custom MATLAB script. Apparent backscatter intensity values were obtained for all images around the heart and data were aligned around the axis of rotation. The data was processed to generate a 3D fiber map of the rat hearts using the intensity relationship (Eq. 1) found above. Data from missing views (i.e. views in between the 10º rotational increments) were interpolated from the acquired views as described in (Milne, et al. 2012).

In vivo Imaging and 3D acquisition

Two rats were used to evaluate the viability of in vivo imaging. In vivo imaging was acquired under isoflurane anesthesia (3% induction, 1–1.5% maintenance) with core (rectal) body temperature maintained at 35°C; heart rate and ejection fraction were measured at ~400bpm and 58%, respectively. Long and short axis B-mode images were acquired with RF-mode active. In one rat, a proprietary 3D acquisition mode (Visualsonics 3D-Mode) with respiratory and ECG gating was used to acquire a 3D images of the heart in vivo in a diastolic state. The heart was removed, imaged in both long and short axis views using 3D mode acquisition. Visualization was performed in VevoLab software. The heart was subsequently fixed, as above, and re-imaged in the short and long axis.

Statistics

Data are reported as mean ± standard deviation (SD). Data analysis and curve fitting were performed in Microsoft Excel (Microsoft Corporation, Redmond, WA); the Solver add-in was used to minimize chi-squared to obtain the curve fit parameters for Eq. 1.

RESULTS

Quantitative Relationship Between Ultrasonic Backscatter and Fiber Angle

We first analyzed apparent ultrasonic backscatter from transmural, cylindrical core samples from the same hearts. Figure 2A shows an example of this data over 90°. The Visualsonics Vevo systems have two modes of operation, a standard mode, which stores data in 8-bit format, and a Digital RF-Mode, which stores data in a 32-bit format. Figure 2B shows the RAW data acquired using standard 8-bit acquisition from 7 transmural core samples, along with the mean and standard deviation of that data. The relationship between apparent backscatter intensity and angle of insonification was fit to Eq. 1, resulting in the following parameters C_1=131.5; C_2=65.8; and C_3=−17.3 for the 8-bit acquisition. Figure 2C shows the RAW data acquired using Vevo Digital RF-Mode 32-bit acquisition from the same 7 samples. The relationship between apparent backscatter intensity and angle of insonification was fit to Eq. 1, resulting in the following parameters C_1=59.6; C_2=14.2; and C_3=−7.1 for the 32-bit acquisition. The difference in the 8-bit verses 32-bit data causes a scaling of the data by 4 (which is equal to the log of the ratio of the data sizes: $\log_{10}(2^{32}/2^8)$). After scaling and offsetting the 8-bit fit parameters C_1=57.5; C_2=65.8/4=16.5; and C_3=−17.3/4=−4.3), we see small deviations between the two acquisitions, but both fits are within the error of the data, suggesting no fundamental variation in the data is associated with the data format choice.

Apparent Ultrasonic Backscatter vs Histological-Image Measured Angle

Ultrasonic images and histological slices were obtained in roughly identical slices parallel to the epicardial wall, transmurally from the epicardium to the endocardium (Fig. 3A). Myocardial fiber angle relative to the circumferential plane was measured from histological images. The data was plotted against the transmural position (Fig. 3B).

Images of histological slices were aligned to ultrasound images so that the apparent ultrasonic backscatter intensity could be compared with the fiber angle corresponding to the same region of an ultrasonic image. The fiber angles were quantified relative to the angle of insonification. These data produce a nearly symmetric relationship between apparent backscatter and fiber angle, with a maximum backscatter near 90º (Fig. 3C).

The histology-validated relationship between apparent backscatter intensity and angle of insonification agreed with the relationship of the core data. Histological data independently fit to Eq. 1 resulting in the following parameters C_1=133.31; C_2=53.4; and C_3=−18.2 with a root mean squared error (RMSE) of 5.97. However, by varying the amplitude of the core fit, we were able to reduce the RMSE to 4.85; fit shown in Figure 4 using C_1=124.7; C_2=65.8; and C_3=−17.3.

Ultrasound-Derived Myocardial Fiber Map and 3D imaging

Reconstructed three-dimensional fiber maps are shown in Figure 5. Comparison between long and short axis measurement of fiber orientation is shown in Figure 6. Evaluation of 3D mode imaging in ex vivo and in vivo conditions is shown in Figure 7.

DISCUSSION

In this study, ultrasound (specifically apparent backscatter) was used to characterize the myofiber architecture in rat hearts. These data show that myocardial fiber mapping is feasible in rat hearts and that the fiber angles determined by ultrasound are consistent with the fiber angle of corresponding histology slices.

Myofiber architecture defines a number of aspects of cardiac mechanics and function. For example, cardiomyocytes shorten by approximately 15% or less in a normal heart (Ingels 1997, Sallin 1969, Streeter and Hanna 1973). A helical alignment allows this modest shortening to translate to ejection fractions upto 100% in theory (Sallin 1969). In addition to a helix, the left ventricular architecture also includes circumferential fibers, which maximally transfer wall tension into blood pressure (Ingels 1997). Physical properties are now being recognized as important aspects of physiologic cardiac function; for example that the helix-ring-helix fiber architecture helps define myocardial torsion (Buckberg, et al. 2008).

Previously, we validated that apparent ultrasonic backscatter could be used to map myofiber architecture in human-size sheep hearts using a clinical imaging system (Milne, et al. 2016). The increase in pre-clinical studies, including a number of rat models of heart failure, suggest numerous opportunities to apply this method in rodents. However, the small scale (mm scale wall thickness, etc) prohibits the use of standard clinical imaging systems. Here, we assessed the viability of using a high frequency (21 MHz) small animal ultrasound system to reconstruct the myocardial fiber architecture in rat hearts.

Rat Myocardial Fiber Anisotropy by Ultrasound

We first confirmed that anisotropy could be imaged and quantified in rat myocardium. The effects of tissue anisotropy on apparent ultrasonic backscatter are clearly evident in Figure 2A. Our quantification (Fig. 2B, C) shows a clear angle-dependent relationship between apparent backscatter and fiber orientation in rat cardiac tissue. In this case, the available imaging modes (with and without Digital RF-Mode) only clearly differed by a scale and offset. The consistency between two modes allow researchers to perform measurements using either mode. These data from rotated myocardial core samples indicate that the relationship between apparent ultrasonic backscatter and myofiber orientation (angle relative to the direction of insonification) is consistent.

To validate that the apparent ultrasonic backscatter intensity does specifically reflect myofiber orientation, we compared ultrasonic data to matched histology data. Previous studies (Milne, et al. 2012, Milne, et al. 2016) have shown that maximum apparent backscatter is associated with a perpendicular relative myofiber orientation and minimum apparent backscatter is associated with a parallel myofiber orientation. For our core data

(Fig. 2), the peak backscatter was similarly assumed to be generated from myofibers oriented 90° relative to the angle of insonification, but the cylindrical symmetry of the core sample meant it was not feasible to histologically reference this sample. Using a trapezoidally shaped sample from the same hearts, we performed a sample-by-sample comparison between histologically determined fiber orientation and ultrasonic backscatter. Our measurements of the fiber angle through the transmural thickness (Fig. 3B) is consistent with previous reports of myofiber orientation in rodents (Lee, et al. 2012, Smith, et al. 2008). These data confirm that myofiber orientation is modified transmurally through the LV wall. By aligning our histological images with ultrasonic images, we re-created a clear relationship between apparent ultrasonic backscatter and the relative myofiber orientation.

Importantly, the relationship between ultrasonic backscatter and myofiber orientation was consistent between core-measured and histologically-validated data. We did find small differences between the coefficients of the fits to Eq. 1, but it is likely that one source of this discrepancy is the lack of data near 0° or 180° relative to the angle of insonification in the trapezoidal wedge data. The strong agreement between the histology data and the relationship (with a constant offset) predicted by the core-data is clear (Fig. 4). These data support the hypothesis that attenuation of the apparent ultrasonic backscatter tissue in myocardium is dependent on myofiber orientation. A likely explanation of the offset is simply the attenuation of the signal at the center of the thicker histological segment, compared to the attenuation at the center of the smaller diameter myofiber core.

Myocardial Fiber Architecture in the Whole Heart

A number of other methods have been proposed to measure the myocardial fiber architecture of rodent hearts, but most are not feasible for in vivo studies. In humans, MRI based DTI measurements are considered state of the art, are feasible, and can give time resolved changes in myofiber architecture (Mekkaoui, et al. 2012, Stoeck, et al. 2014, von Deuster, et al. 2016). In rodents however, the rapid heart rate and long acquisition times are prohibitive (Zhang and Wei 2017). Similarly, other methods to measure fiber architecture, such as optical coherence tomography, requires explant of the hearts (Castonguay, et al. 2017). Other quantitative ultrasound measures of fiber architecture, such as backscatter tensor imaging (Papadacci, et al. 2017), require 2D arrays, have either only been validated in large animals, and/or are more computationally complex.

Using ultrasound, specifically apparent ultrasonic backscatter, has a number of advantages over other methods such as DTI. First, our method can be used by calibrating any standard clinical ultrasound unit. Second, an ultrasound method that is scalable (such as our method) is useful for quantifying myocardial fiber architecture in patients where MRI might be contraindicated. Examples where DTI might not be feasible include: neonatal pediatric imaging or adult heart failure, where electronic device such as left ventricular assist devices (LVAD) and pacemakers are often present.

Based on the data from the core and the histologically-validated wedge samples, we also performed a 3D reconstruction of a whole heart (Fig. 5). These data suggest that reconstruction of the myofiber architecture of rodent hearts is feasible and that the myofiber orientation produces a predictable change in apparent backscatter.

This study was also designed to mimic a similar study (Milne, et al. 2016) in that it reconstructed 3D images from a series of 2D apical images. Imaging in rodents is more difficult than in humans due to the location of rodent hearts in the chest and the small rib spacing, especially for apical imaging. Short-axis imaging may provide an alternate view for in vivo measurement of myocardial fiber architecture in rodents, but rib and lung shadowing can interfere with a full 3D reconstruction (Fig. 6A, C). Nonetheless, the methods described here can be used for any imaging plane, with the caveat that fibers perpendicular to the angle of insonification would be difficult to quantify. Figure 6E–G shows a comparison between backscatter estimates in long axis vs short axis images. Deviation from the predicted angles are likely due to the difficulty in aligning the heart axis.

Unlike clinical imaging probes, high frequency probes are only available in single element or linear array format. In vivo 3D image acquisition can be performed using motor control (Vevo3D). Initial testing suggests that 3D images acquired using this method represent the expected anisotropy in apparent backscatter (Fig. 7) and the ultrasound fiber mapping can be applied to such images. This method could be used both ex vivo and in vivo. The validation that we are performing in rodents also opens up an important arena to use pre-clinical models to study how the myofiber architecture changes in disease (Buckberg, et al. 2004).

Limitations

This method currently uses the ultrasonic voxel as an individual region of interest and treats each voxel as a discrete region of interest. DTI methods allowed tracking of diffusion along fiber tracts, much larger than the region of interest (Mekkaoui, et al. 2012). This fiber tract method appears to improve the ability of DTI to replicate histologically-measured fiber angles. Including fiber tracts as a means of joining voxels may refine fiber maps, mitigating the effects ultrasonic speckle or other noise which may cause a voxel to generate unusually low or high backscatter.

The relationship between apparent ultrasonic backscatter and angle of insonifcation is symmetric around 90°, meaning the backscatter itself cannot identify the helix direction of the fiber angle. However, nearly all hearts appear to hold the same counterspiral angles where the endocardial fibers following a right hand helix and epicardial fibers following a left hand helix (Streeter and Hanna 1973). (Even in situs inversus totalis, the fiber helix is thought to be follow the same helix-handedness (Delhaas, et al. 2008)). Thus, it can generally be assumed that the direction of the helix and fiber angles can be inferred from the transmural position in the heart.

In this study, we used only a single sex of animal (females) to minimize the biological variables impacting our results. Preliminary studies comparing the relationship between backscatter and fiber angle using cylindrical cores from male and female rats (not shown) suggest that this is not a relevant biological variable for this relationship. A detailed study evaluating the effects of biological variables such as sex is merited.

Conclusion

Apparent backscatter was successfully used to measure myocardial fiber angle in fixed, intact rat hearts. The relationship between fiber orientation and apparent backscatter was

determined using cored sections of the heart walls. Additionally, the relationship between ultrasound and myofiber angle orientation was verified in transmural wedge segments using histology. Ultrasound, specifically apparent backscatter, may provide a feasible and rapid method to measure myocardial fiber architecture in rodents, in addition to in humans.

ACKNOWLEDGEMENTS and SOURCES OF FUNDING

We thank Mark A. Hiske and Melissa J Bukowski for additional data acquisition.

Supported by the American Heart Association (14SDG20100063, 18TPA34170169) to CSC and the Patuxent Partnership to MLM). Funding sources had no involvement in study design; in the collection, analysis and interpretation of data; in the writing of the report; and in the decision to submit the article for publication.

LITERATURE CITED

Buckberg G, Hoffman JI, Mahajan A, Saleh S, Coghlan C. Cardiac mechanics revisited: the relationship of cardiac architecture to ventricular function. Circulation 2008; 118:2571–87. [PubMed: 19064692]

Buckberg GD, Weisfeldt ML, Ballester M, Beyar R, Burkhoff D, Coghlan HC, Doyle M, Epstein ND, Gharib M, Ideker RE, Ingels NB, LeWinter MM, McCulloch AD, Pohost GM, Reinlib LJ, Sahn DJ, Sopko G, Spinale FG, Spotnitz HM, Torrent-Guasp F, Shapiro EP. Left ventricular form and function: scientific priorities and strategic planning for development of new views of disease. Circulation 2004; 110:e333–6. [PubMed: 15466651]

Castonguay A, Lefebvre J, Pouliot P, Avti P, Moeini M, Lesage F. Serial optical coherence scanning reveals an association between cardiac function and the heart architecture in the aging rodent heart. Biomedical optics express 2017; 8:5027–38. [PubMed: 29188099]

Delhaas T, Kroon W, Bovendeerd P, Arts T. Left ventricular apical torsion and architecture are not inverted in situs inversus totalis. Prog Biophys Mol Biol 2008; 97:513–9. [PubMed: 18403001]

Ingels NB Jr. Myocardial fiber architecture and left ventricular function. Technol Health Care 1997; 5:45–52. [PubMed: 9134618]

Kocica MJ, Corno AF, Carreras-Costa F, Ballester-Rodes M, Moghbel MC, Cueva CN, Lackovic V, Kanjuh VI, Torrent-Guasp F. The helical ventricular myocardial band: global, three-dimensional, functional architecture of the ventricular myocardium. Eur J Cardiothorac Surg 2006; 29 Suppl 1:S21–40. [PubMed: 16563790]

Kovacs A, Courtois MR, Weinheimer CJ, Posdamer SH, Wallace KD, Holland MR, Miller JG. Ultrasonic tissue characterization of the mouse myocardium: successful in vivo cyclic variation measurements. J Am Soc Echocardiogr 2004; 17:883–92. [PubMed: 15282494]

Lee WN, Pernot M, Couade M, Messas E, Bruneval P, Bel A, Hagege AA, Fink M, Tanter M. Mapping myocardial fiber orientation using echocardiography-based shear wave imaging. IEEE Trans Med Imaging 2012; 31:554–62. [PubMed: 22020673]

Mekkaoui C, Huang S, Chen HH, Dai G, Reese TG, Kostis WJ, Thiagalingam A, Maurovich-Horvat P, Ruskin JN, Hoffmann U, Jackowski MP, Sosnovik DE. Fiber architecture in remodeled myocardium revealed with a quantitative diffusion CMR tractography framework and histological validation. J Cardiovasc Magn Reson 2012; 14:70. [PubMed: 23061749]

Milne ML, Singh GK, Miller JG, Holland MR. Echocardiographic-based assessment of myocardial fiber structure in individual, excised hearts. Ultrason Imaging 2012; 34:129–41. [PubMed: 22972911]

Milne ML, Singh GK, Miller JG, Wallace KD, Holland MR. Toward 3-D Echocardiographic Determination of Regional Myofiber Structure. Ultrasound Med Biol 2016; 42:607–18. [PubMed: 26589530]

Mizuguchi Y, Oishi Y, Miyoshi H, Iuchi A, Nagase N, Oki T. The functional role of longitudinal, circumferential, and radial myocardial deformation for regulating the early impairment of left ventricular contraction and relaxation in patients with cardiovascular risk factors: a study with two-dimensional strain imaging. J Am Soc Echocardiogr 2008; 21:1138–44. [PubMed: 18926389]

Health Research Alliance Author Manuscript

Mottley JG, Miller JG. Anisotropy of the ultrasonic backscatter of myocardial tissue: I. Theory and measurements in vitro. J Acoust Soc Am 1988; 83:755–61. [PubMed: 3351133]

Papadacci C, Finel V, Provost J, Villemain O, Bruneval P, Gennisson JL, Tanter M, Fink M, Pernot M. Imaging the dynamics of cardiac fiber orientation in vivo using 3D Ultrasound Backscatter Tensor Imaging. Sci Rep 2017; 7:830. [PubMed: 28400606]

Sallin EA. Fiber orientation and ejection fraction in the human left ventricle. Biophys J 1969; 9:954–64. [PubMed: 5791550]

Smith RM, Matiukas A, Zemlin CW, Pertsov AM. Nondestructive optical determination of fiber organization in intact myocardial wall. Microsc Res Tech 2008; 71:510–6. [PubMed: 18393296]

Stoeck CT, Kalinowska A, von Deuster C, Harmer J, Chan RW, Niemann M, Manka R, Atkinson D, Sosnovik DE, Mekkaoui C, Kozerke S. Dual-phase cardiac diffusion tensor imaging with strain correction. PLoS One 2014; 9:e107159. [PubMed: 25191900]

Streeter DD Jr., Hanna WT. Engineering mechanics for successive states in canine left ventricular myocardium. II. Fiber angle and sarcomere length. Circ Res 1973; 33:656–64. [PubMed: 4762007]

von Deuster C, Sammut E, Asner L, Nordsletten D, Lamata P, Stoeck CT, Kozerke S, Razavi R. Studying Dynamic Myofiber Aggregate Reorientation in Dilated Cardiomyopathy Using In Vivo Magnetic Resonance Diffusion Tensor Imaging. Circulation. Cardiovascular imaging 2016; 9.

Zhang YY, Wei HJ. Atlas construction of cardiac fiber architecture using a multimodal registration approach. Neurocomputing 2017; 259:219–25.

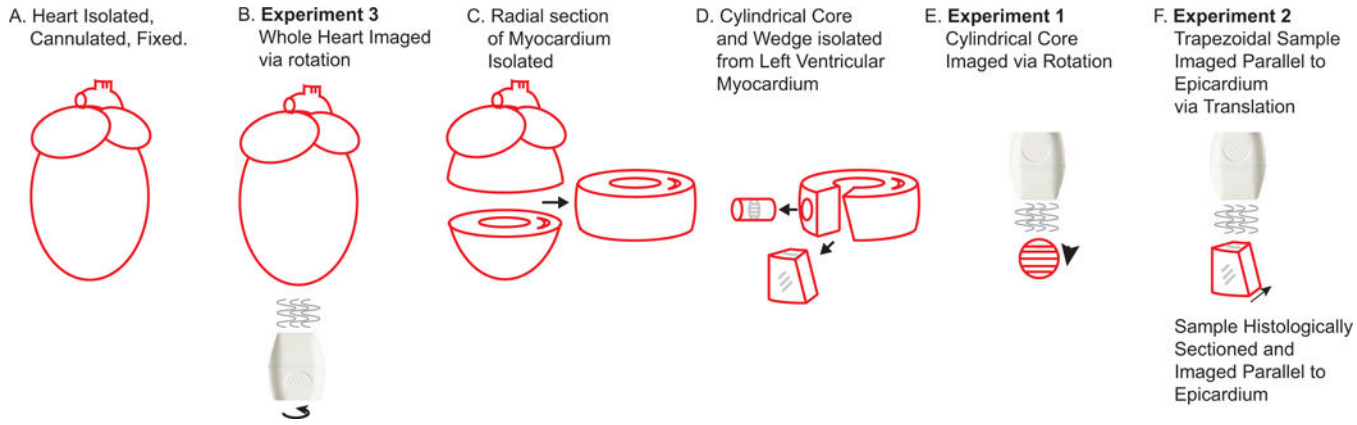

Figure 1. Methods Overview.

Processing of rat heart samples. First, hearts were prepared for imaging (A). Whole, fixed hearts were then imaged ultrasonically in long-axis views with the transducer placed near the apex (B). The heart was rotated in 10 degree steps in order to capture data from the entire heart. After whole-heart imaging, a radial section of the heart was selected (C) and a wedge and core were isolated from the section (D). The core was imaged across the short axis, with images taken while the core was rotated in 5 degree increments in order to vary the fiber direction relative to the ultrasound insonification direction (E). The trapezoidal wedges were ultrasonically imaged serially through the myocardial thickness then prepared for histologically in order to compare fiber orientation obtained from ultrasound and orientation obtained from histology. For most hearts, all steps (A–F) were performed. Experimental data were performed in steps E, F, and B as described in the methods.

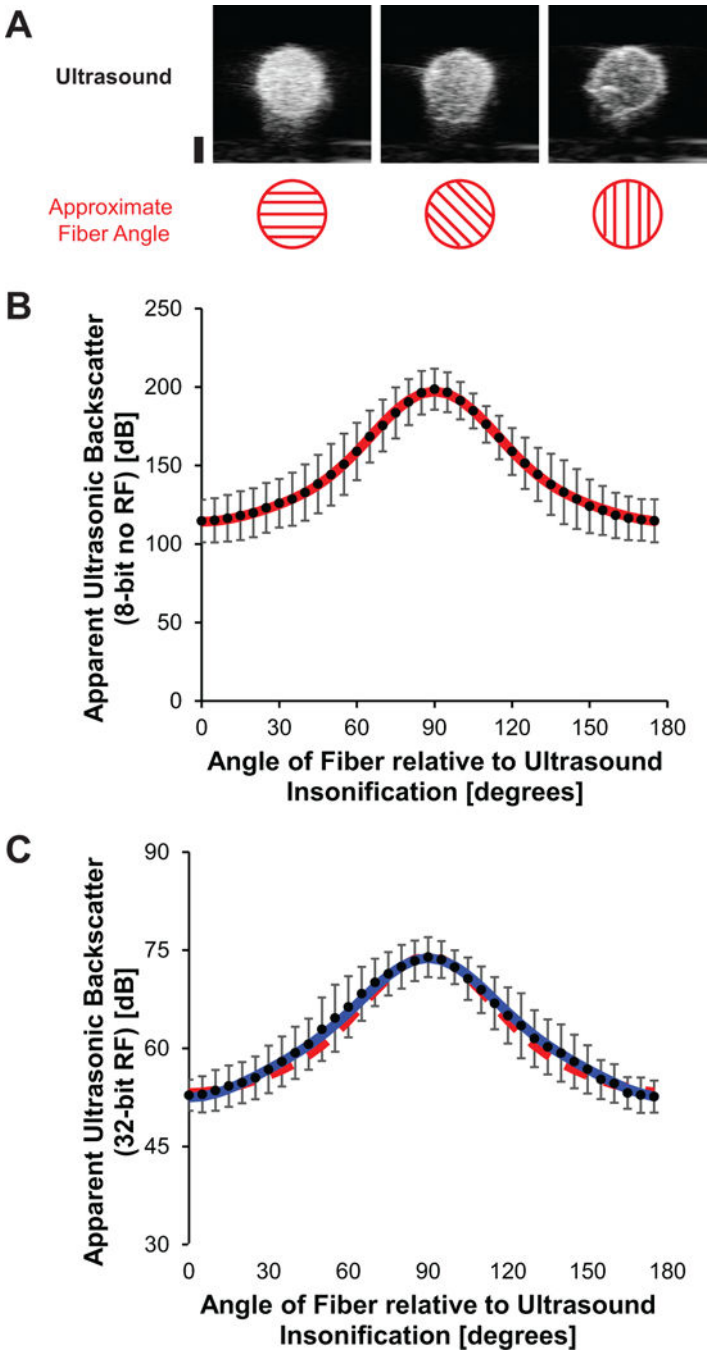

Figure 2. Relationship between apparent ultrasonic backscatter intensity and angle of rotation in cylindrical myocardial tissue cores.

Data acquired using VisualSonics Vevo2100 with MS250D transducer at 21 Mhz with a receiver gain of 60 dB at 100% transmit power. A) Example ultrasound core images at minimum backscatter amplitude, rotated 45° from minimum and rotated 90° from minimum (which was peak backscatter). Maximum backscatter was assigned a fiber angle of 90^{o} between the fiber orientation and the insonification angle. Black bar at lower left of image denotes 1 mm. B) Relationship between apparent ultrasonic backscatter and fiber orientation using standard (8 bit) acquisition without Vevo Digital RF-Mode in n=7 samples. Fit (red

curve) shown over mean±SD (black circle, bars) for data without RF. C) Relationship between apparent ultrasonic backscatter and fiber orientation using Vevo Digital RF-Mode (32-bit) acquisition in n=7 samples. Fit (blue curve) shown over mean±SD (black circle, bars) for data with RF. The fit parameters (C_2, C_3) from the non-RF data (red dashed curve) were scaled by 4 ($\log_{10}(2^{32}/2^{8})$) and offset (C_1), showing strong overlap between the data points, suggesting no significant difference in data gathered in the two modes.

Health Research Alliance Author Manuscript

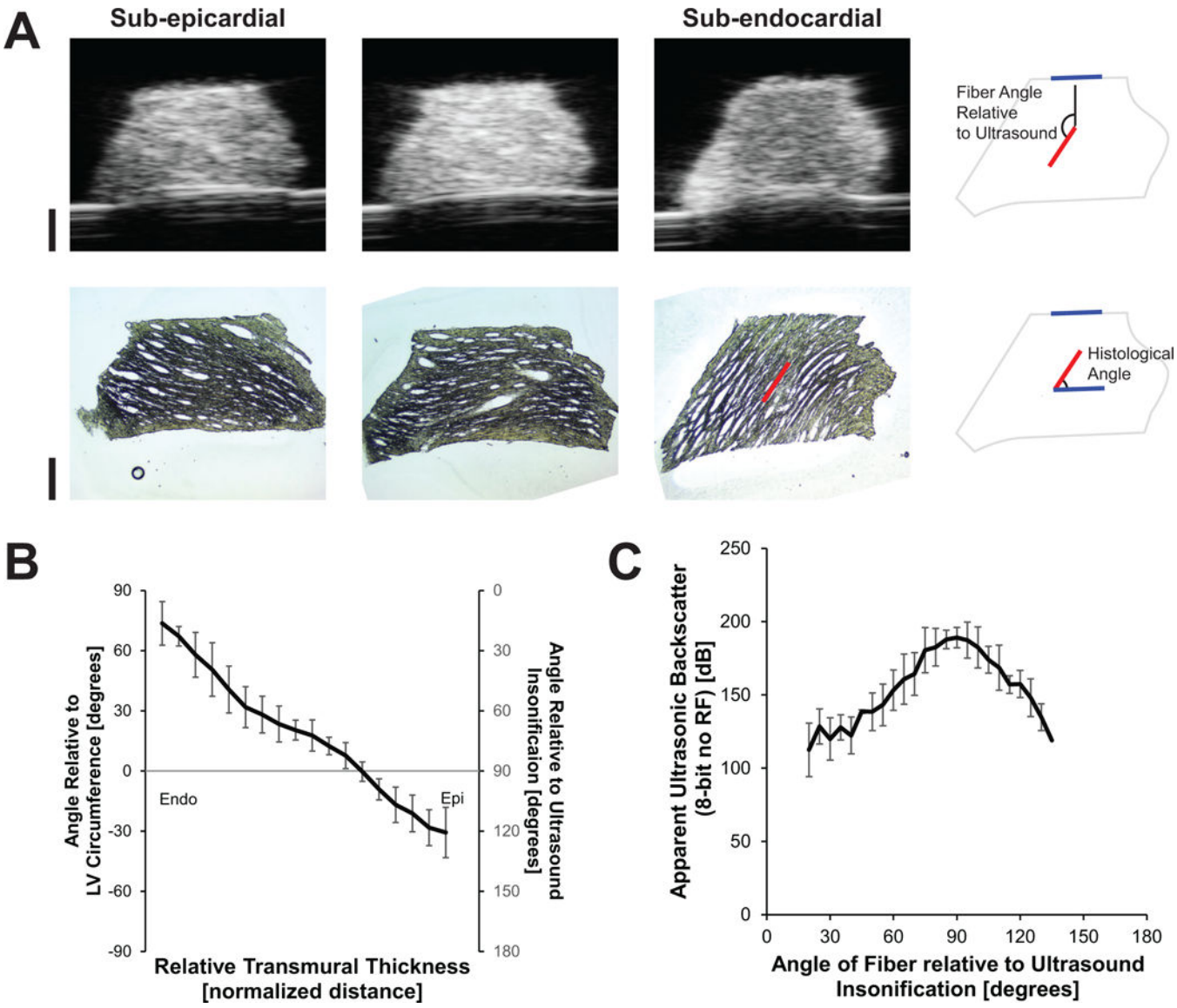

Figure 3. Histological angle and apparent ultrasonic backscatter from myocardial wedge preparations.

A) Ultrasound (top) and histological sections (bottom) from a single heart. The figures on the right show an example of how angles were calculated using the fiber angle (red line) in the endocardial image. Ultrasound TIFF exported images shown (C5 color map); histological images scaled and rotated, no other image manipulations were performed. Black bars at left denotes 1 mm. At right, references to the measured angles are shown; the user aligned the tops of the ultrasound and histology images (blue lines) for reference. B) Measured histological fiber orientation (mean±SD, n=7) versus relative transmural position though the heart, which replicates previously published data (see Discussion for details); the angle relative to the insonification direction is shown on the right side of the graph. C) Relationship between histological angle (mean±SD, n=7) and ultrasonic backscatter in myocardial tissue segments. Endocardial data is plotted at the left (with lower relative

angle), epicardial data towards the right (higher relative angle). Note the similarity to Figure 2, which showed the ultrasonically-determined angle and backscatter.

Health Research Alliance Author Manuscript

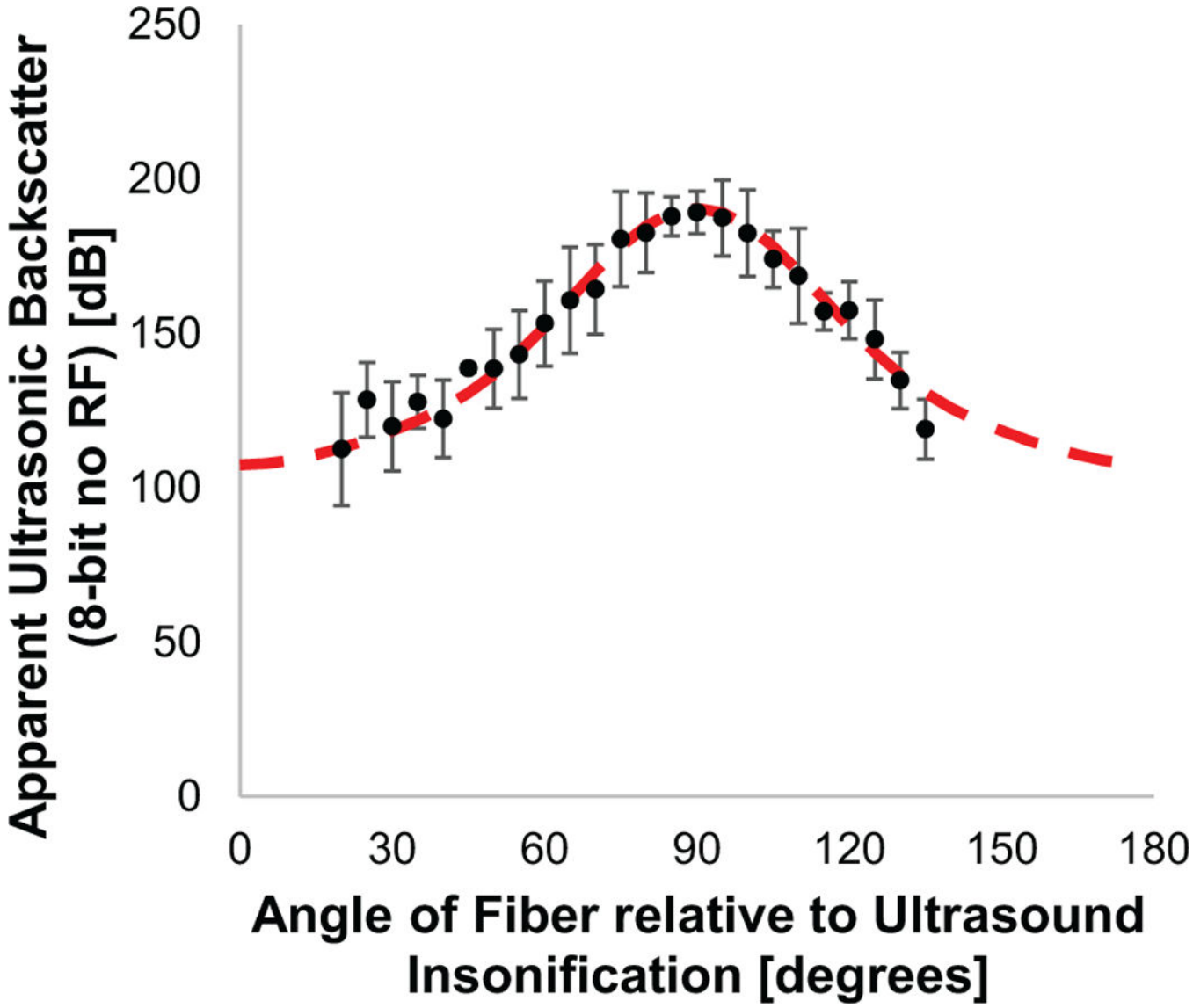

Figure 4. Comparison of histology-validated data fit and core data fit.

Data from the comparison of histology and ultrasound Figure 3C (black circles and standard deviation error bars) overlaid with the relationship (red dashed curve) determined in Figure 2B, offset to account for attenuation. Note the strong agreement between the two methods of determining fiber orientation. Endocardial data is plotted at the left (with lower relative angle), epicardial data towards the right (higher relative angle).

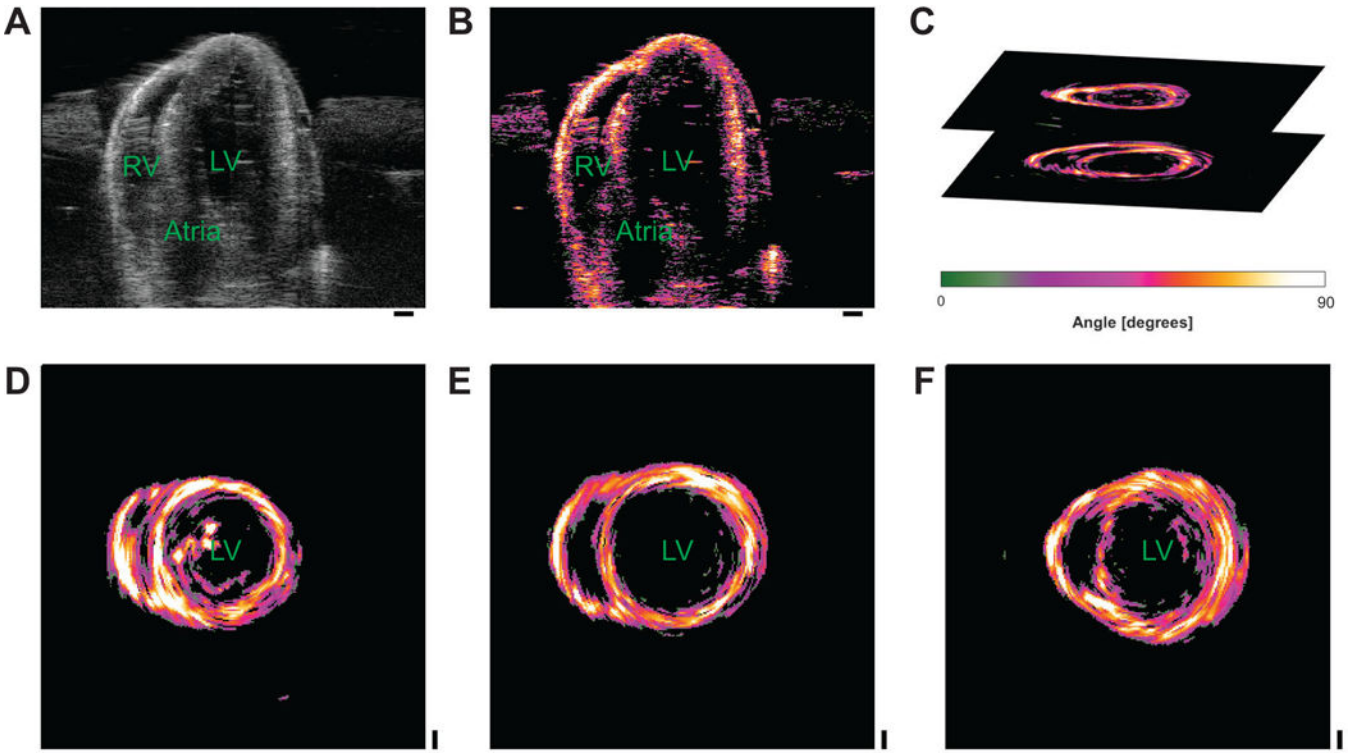

Figure 5. 3D myocardial fiber mapping of a rat heart.

A) B-mode ultrasound image reconstructed and scaled based on apparent backscatter acquired in RF-mode from one rat heart. Note, horizontal backscatter near the top of the image are surface effects from the imaging stage. B) Same image as panel A, mapped to myofiber orientation. Note the bright white near the mid-myocardium of the left ventricle denoting circumferential fibers, perpendicular to the direction of insonification (top to bottom). C) Two short-axis plots reconstructed from B-mode images, roughly aligned to their vertical position in Panel B. Color bar for Panels B–F shown at the bottom of Panel C. D–F) Example reconstructed short axis myocardial fiber architecture near the mid-myocardium of 3 additional rat hearts. Black bar on lower right hand side of images denote 1 mm.

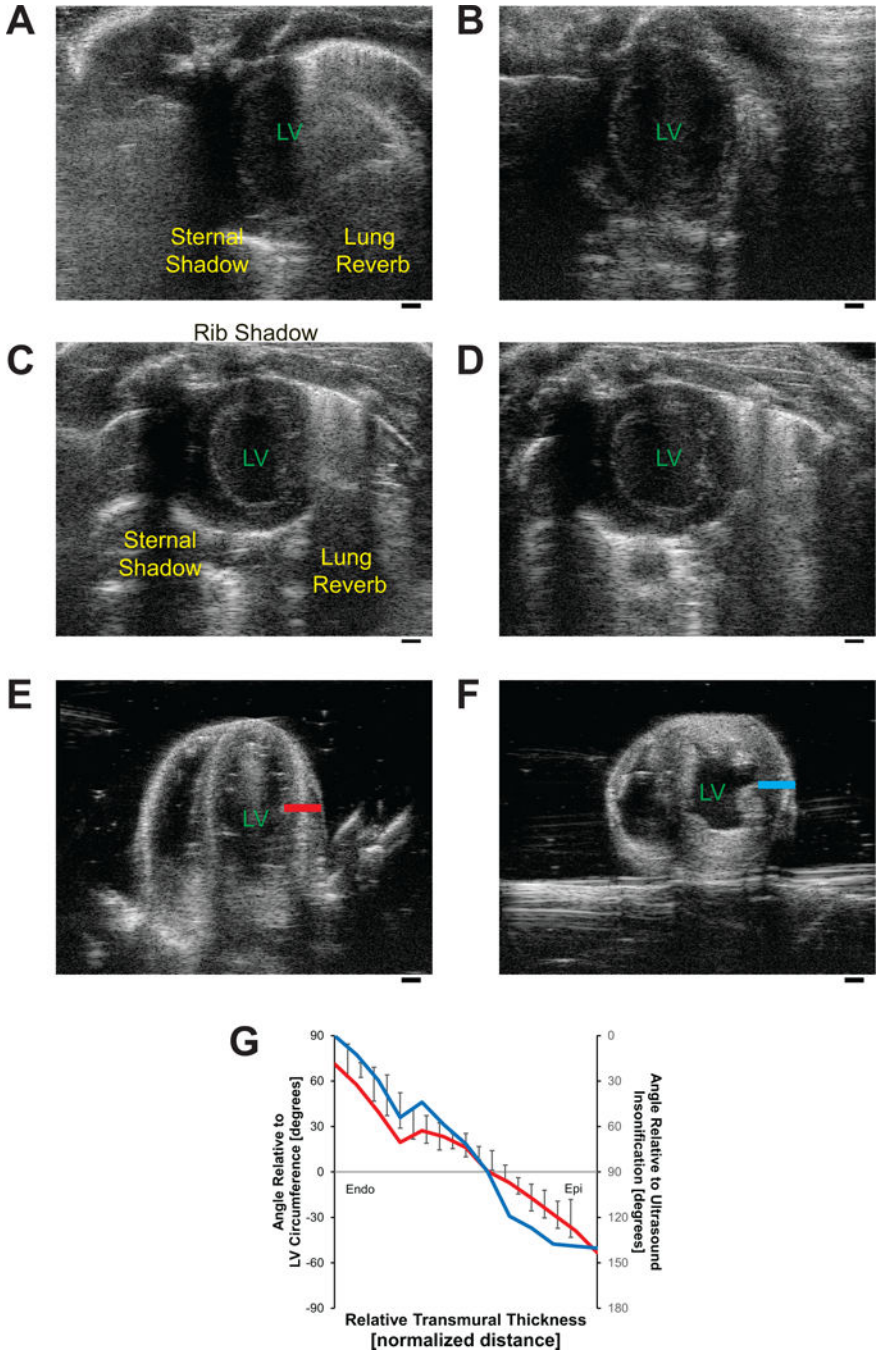

Figure 6. Considerations for in vivo fiber mapping.

A–D) In vivo long- and short-axis imaging in a rat. Both views can suffer from shadowing from ribs and the sternum or reverberations from the lungs (A, C). The long axis can be more difficult in the rodent, causing signal drop out (B), so short axis views may be necessary to perform measurements. The RV, always plotted to the left, is often hidden by shadowing. E) Long- and F) short-axis imaging of a fixed ex vivo rat heart. (Note, ex vivo and in vivo images were taken from different rats.) Black bar on lower right hand side of images denote 1 mm. G) Comparison between reconstructed myofiber orientation across the

transmural wall of the heart from Panel E (red bar) and Panel F (blue bar). Ultrasound predicted myofiber orientation (red, blue) lines shown with the standard deviation range of the histologically-measured values (black) taken from Figure 3.

Health Research Alliance Author Manuscript

Health Research Alliance Author Manuscript

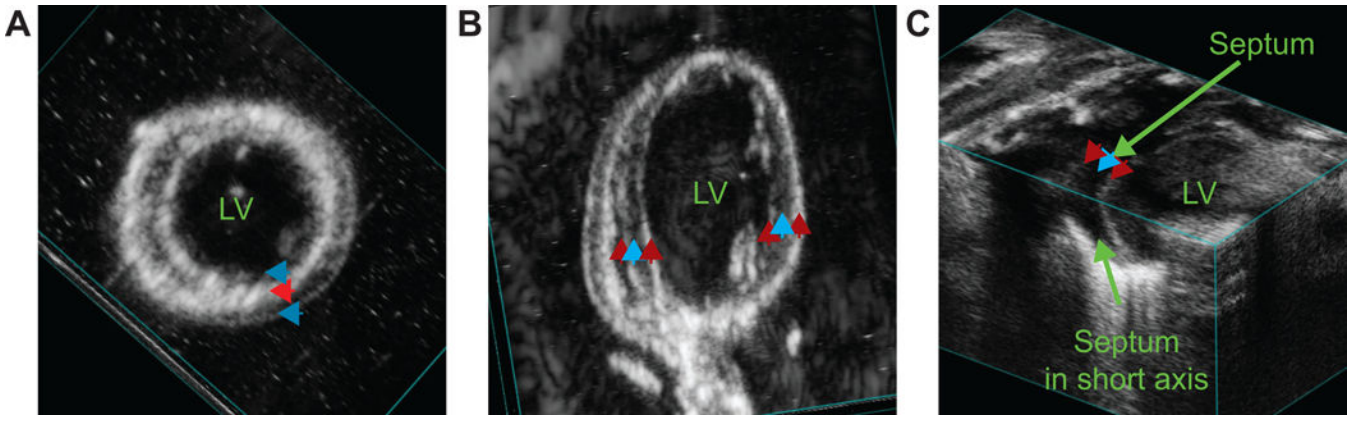

Figure 7. 3D imaging.

Example ex vivo 3D apparent backscatter imaging in the A) long and B) short axes. Images represents cutaway of the 3D image perpendicular to the angle of insonification, which is roughly in/out of the page. C) Example in vivo imaging in the short axis. Image shows a cutaway of the 3D image. The front (bottom left) is in line with a short axis image; the top is a cutaway roughly perpendicular to the angle of insonification, which is parallel to the vertical blue line that denotes a corner of the cutaway. Myofiber orientation (roughly) parallel or perpendicular to the angle of insonification are denoted by red or blue arrows respectively.